J Therm Spray Tech
https://doi.org/10.1007/s11666-019-00865-1

PEER REVIEWED

Fatigue Bending Behavior of Cold-Sprayed Nickel-Based Superalloy Coatings

A. Silvello[1,3] · P. Cavaliere[1] · A. Rizzo[2] · D. Valerini[2] · S. Dosta Parras[3] · I. Garcia Cano[3]

Submitted: 11 October 2018 / in revised form: 22 February 2019

Abstract Cold-sprayed Ni-based superalloy coatings offer new possibilities for manufacturing and repairing damaged components, such as gas turbine blades or other parts of aircraft engines. This development shines a new light on the conventional additive manufacturing technologies and significantly broadens application fields of cold spray. The idea is that cold spray can contribute to improving the fatigue properties of manufacturing and repaired components. This study deals with the analysis of the microstructural and mechanical properties of IN625 cold-sprayed coatings on V-notched carbon steel substrate. Process conditions of 1000 °C and 50 bar were employed to produce coatings in V-notched (60° and 90°) samples in order to evaluate the fatigue crack behavior of the sprayed material. Bending tests were carried out in order to evaluate the crack propagation in the coatings during cyclic loading. The K factor was quantified for the two different notch geometries. After fatigue tests, the cracking mechanisms were observed through SEM. Optical microscopy, nanoindentation as a function of coating/substrate distance and corrosion tests were performed. Porosity measurements through image analyses were done to characterize the coatings' quality. The results achieved demonstrate that cold spray deposition and repair can contribute to resistance and to the increase in the global fatigue life of cracked structures.

Keywords cold spray · fracture behavior · IN625, fatigue · superalloys

✉ P. Cavaliere
pasquale.cavaliere@unisalento.it

[1] Department of Engineering for Innovation, University of Salento, 73100 Lecce, Italy

[2] ENEA, Italian National Agency for New Technologies, Energy and Sustainable Economic Development, SSPT-PROMAS-MATAS, S.S. 7 Appia, km 706, Brindisi, Italy

[3] Thermal Spray Centre, CPT, Universitat de Barcelona, 08028 Barcelona, Spain

Introduction

Cold spray (CS) is no longer restricted to prototyping, but establishes itself as manufacturing technology for functional parts with properties comparable to conventionally manufactured components (Ref 1-3). The high kinetic energy of particles enables a strong particle/particle and particle/substrate bonding and consequently creates solid coatings with a density larger than 99.5% (Ref 4, 5). Conventional thermal spray processes are widely used in many applications to do coatings, but thermal energy can melt or soften the feedstock powders. This can cause thermal degradation and partial oxidation of the coating material which may be undesirable. For metallic materials that are very prone to oxidation, thermal spray needs to be conducted under a protected atmosphere or a vacuum, introducing extra cost. Moreover, thermal energy can induce phase transformation. For example, after long thermal exposure, most common Ni-based superalloys are susceptible to the δ phase formation that can evolve during processing or during service. Ni-based superalloys that are precipitation-strengthened by the γ'' phase are susceptible to δ phase formation, which can evolve during processing or during service (Ref 6, 7). The δ precipitates normally have a plate morphology though globular particles have also been observed (Ref 6). It has been reported that the formation of δ precipitates can occur at the austenite grain boundaries at relatively low temperatures and in an

Published online: 06 May 2019

intragranular fashion at relatively high temperatures. Controlled δ precipitation appears to have a beneficial effect on stress rupture ductility. However, the formation of a large amount of coarse δ plates degrades the strength of γ'' hardened superalloys. On prolonged exposure at intermediate temperatures, the δ phase forms as a transformation product of γ'' phase (Ref 6-9). δ, μ and Laves phases have low ductility and cause losses in mechanical and corrosion properties (Ref 10). This potential recently accelerated the introduction of CS as an alternative to conventional manufacturing technologies in the aircraft, automotive and biomedical sectors. Due to high specific strength and corrosion resistance, the Ni-based superalloys are in particular interest for designs in aerospace applications. Furthermore, the high demand for quality and structural integrity in this industry requires a detailed investigation on the fatigue behavior of CS manufacture. CS and additive manufacturing (AM) processes have been made possible to deposit and print metal parts and components, making it a potentially disruptive innovation for manufacturing sector. Of course, the challenge is to reduce the gap between the quality of components created by CS and AM processes and those created through traditional manufacturing processes. For example, there is a lack of information related to coatings' properties after deposition and there is a lack of information related to different coating/substrate combinations. In a previous work (Ref 11), we have seen how the same Ni-based superalloy powder sprayed on two different substrates (C steel and Al) with the same process setup achieved two different porosity levels. Coating porosity level on Al substrate was almost 10 times greater than coating porosity level on C steel substrate. Porosity is strongly dependent on sprayed material and processing parameters. Most of the mechanical properties of the coatings become degraded along with the increase in porosity because pores in the coating layer eventually mean unbonded interparticle interface. Moreover, it has been seen that corrosion travels through pores of the coating, and hence, porosity plays a very important role to resist again corrosion (Ref 12), because porosity acts as a transport conduit for corrosive solution. Besides, other authors use CS as an emerging coating technology to protect, fabricate and restore components. Henao et al. (Ref 13) used Al-based metallic glass coatings to protect Al alloys in corrosive and wear environments. Yin et al. (Ref 14) used it to fabricate rotational and net-shape structure and to restore aircraft component. Damages frequently occur in service due to corrosion, wear and fatigue and have to be replaced due to the lack of effective restoration methods. In this paper, IN625 is used for its outstanding corrosion resistance, high strength and excellent fabricability (including joining). Strength of IN625 is derived from the stiffening effect of Mo and Nb on its nickel/chromium matrix; thus, precipitation-hardening treatments are not required. The properties of IN625 are free from pitting and crevice corrosion, high corrosion fatigue strength, high tensile strength and resistance to chloride-ion stress corrosion cracking. High tensile, creep and rupture strength, outstanding fatigue and thermal fatigue strength, oxidation resistance and excellent weldability and brazeability are the properties of IN625 that make it interesting to different industrial sectors, such as chemical and petrochemical plants, power generation sector, aircraft engines components, heat exchanger tubing or boilers of waste incinerators (Ref 15, 16). About fatigue properties and crack initiation and growth behavior of cold spray coatings, very few papers are presented in the literature, and in particular, very few evidences are presented for Ni-based coatings. Different papers presented the fatigue behavior of aluminum alloys structures repaired via cold spray (Ref 17, 18). The positive effect on fatigue properties is dependent on many different spray parameters (Ref 19). Obviously, each material system has different behaviors depending on powder properties, machine conditions and geometries (Ref 20, 21).

In the present study, optimal deposition conditions are employed to produce IN625 coatings in order to evaluate mechanical properties and the crack initiation and growth behavior during fatigue loading.

Experimental Procedure

Cold spray coatings were produced by employing a CGT Kinetics 4000 series machine with a SiC nozzle, with rectangular cross section 2 × 4 mm throat and 2 × 10 mm exit (CPT, Barcelona, ES). IN625 superalloy particles (produced via argon atomization) were sprayed on carbon steel substrates (0.3%). Particles from Sulzer Metco with size − 45 + 15 μm were deposited. Particle chemical composition and particle size distribution are available in Ref 22. The carbon steel sheets measured 50 * 20 * 5 mm. Before process deposition, substrates were sand-blasted with Al_2O_3 up to R_a = 6 μm. The process parameters were temperature (1000 °C), pressure (50 bar), stand off distance (40 mm) and traverse gun speed (500 mm/s). N_2 was used as carrier gas. After process deposition, samples were mounted in epoxy resin, grit-blasted with SiC papers (240, 320, 400, 600 and 1200 grit) and polished with diamond suspension (6 μm and 1 μm). 60° and 90° V-notches of 100 μm depth were machined on the surface of C steel substrates; the notches were filled with cold-sprayed IN625 particles (Fig. 1).

Hardness measurements of coatings as a function of substrate/coating interface were performed by means of nanoindentation using an Anton Paar nanoindenter model

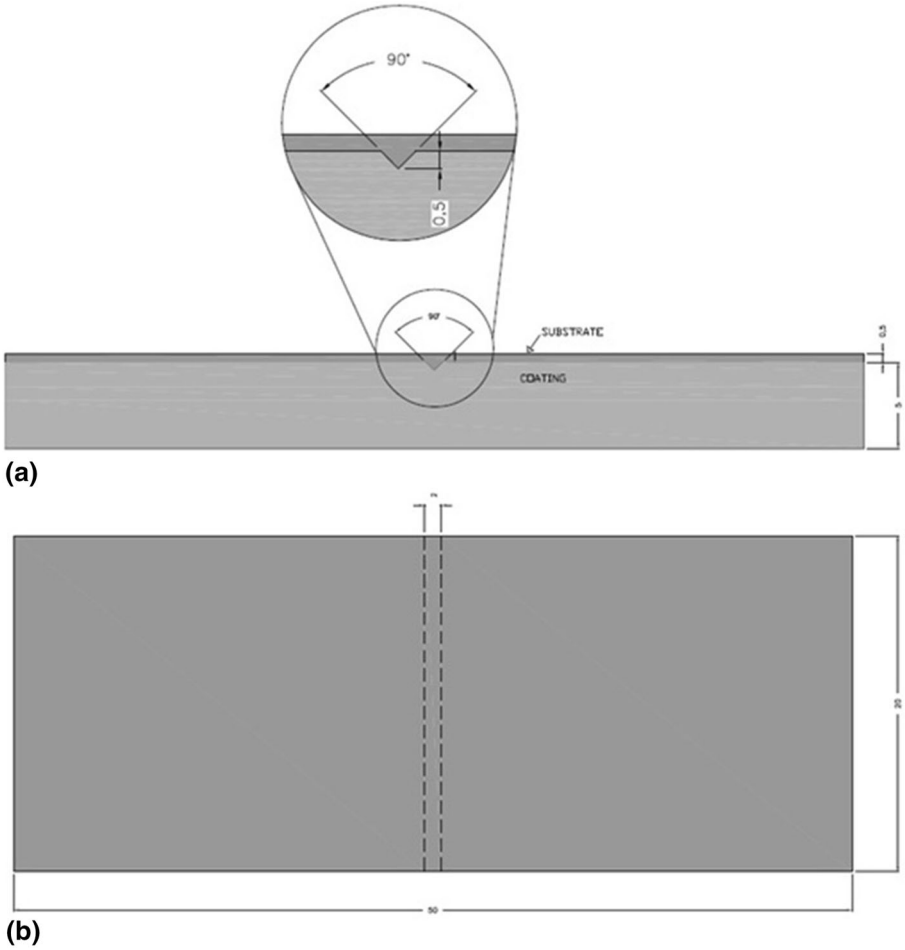

Fig. 1 Notch filled with cold-sprayed particles, transversal section (a); superior view (b)

TTX-NHT2 equipped with a Berkovich diamond indenter. The tests were performed under load control, with an applied maximum load of 50 mN, and the dwell time was 5 s for each indent. The tests were performed under load control; the average values were taken from 20 indentations per sample.

The coatings' residual stresses were evaluated through x-ray diffraction measurements by employing a Rigaku Ultima diffractometer (Ref 23). Then, the coatings' fatigue behavior was evaluated through the three-point bending tests performed up to coating fracture. The crack initiation and growth behavior analysis was performed through the three-point bending cyclic tests performed with a sinusoidal waveform at a frequency of 1 Hz. The tests were performed with Zwick/Roell Z100 standard machine. The maximum load during tests was 3 kN, and the load ratio was $R = 0.1$ for all the tests. The stress intensity factor (K) was calculated based on classical equations and mechanical properties. The classical Paris law was employed for the crack propagation behavior Eq 1.

$$\frac{da}{dN} = C\Delta K^m \qquad \text{(Eq 1)}$$

where a is the crack length, N the number of loading cycles and C and m the constants depending on the material.

The setup of the three-point bending tests is shown in Fig. 2.

The cracks' growth rate was calculated by using a direct current potential drop method (Ref 24). A constant direct current is conducted in the specimen. The amperage is selected according to the material and the dimension of the specimen to avoid critical heating on the specimen. Plastic

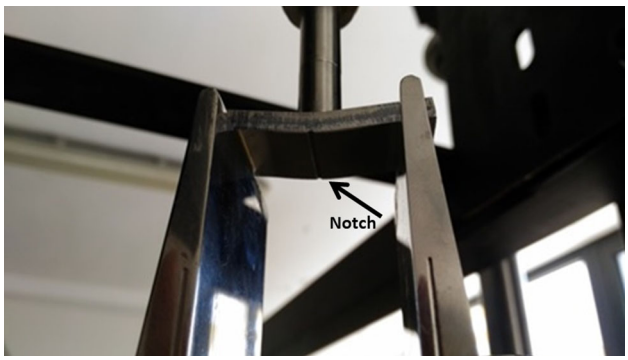

Fig. 2 Three-point bending setup

insulators are mounted on two sides of the specimen-clamping systems to prevent current leakage. Two metal pins are welded onto two sides of the gauge section and connected to a voltmeter to record the potential drop during the test (Ref 25). The potential slightly increases at the beginning of the test due to the progressive reduction of the area of the cross section caused by the incremental loading. At a particular phase of the experiment, due to the appearance of severe discontinuity induced by the coalescence of voids or the formation of microcrack or shear bands, the electrical resistance/potential increases suddenly. This time instant is assumed as the crack initiation and the corresponding force as the critical load. To verify the correct detection of the crack initiation and correlate the response of current potential to the underlying damage mechanisms, some interrupted tests are performed in order to verify the crack length at a fixed electric signal.

The results of the crack behavior were compared with those belonging to the same material sprayed in different conditions and described in a previous paper (Ref 22). The fracture surface observations were performed by employing a Zeiss EVO40 SEM. The coating microstructure was observed by employing the optical microscope Leica DMI 5000M by using an image software analysis, while porosity was measured by employing the ImageJ processing software. For setup process condition, seven porosity measurements were performed. Samples were etched in two different ways for the splatted particle observation through optical microscopy: first immersion in aqua regia (nitric acid/hydrochloric acid in a molar ratio of 1:3) and second immersion in 60 ml glycerol + 50 ml HCl + 20 ml HNO_3. Corrosion was evaluated by electrochemical measurements in 3.5% NaCl solution; a conventional three-electrode cell was used, with an Ag/AgCl as reference electrode, a Pt wire as counter electrode and the as-sprayed samples (1 cm^2) as the working electrode. A PC-programmed EG&G 263A potentiostat/galvanostat (Princeton Applied Research, UK) was employed. For all the specimens, the following procedure was applied: once the open-circuit potential was stabilized, a linear polarization was performed in the small potential range around the open-circuit potential, and finally, the potentiodynamic curves were recorded.

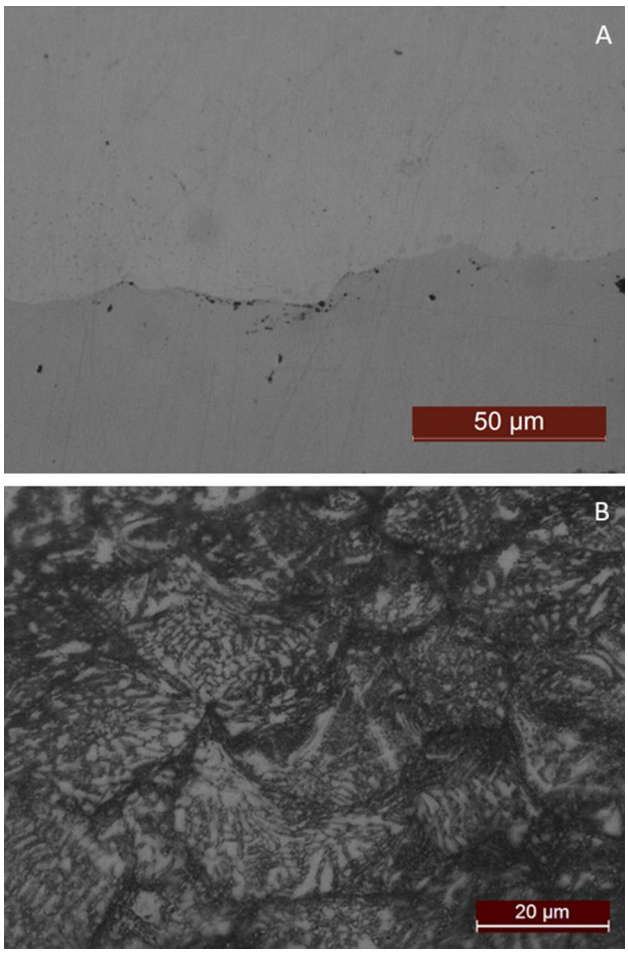

Fig. 3 Optical microstructure of the CSed coatings (a); etched microstructure (b)

Results and Discussion

Evaluation of Mechanical Properties

The coatings' thickness measured a mean value of 391 ± 9 µm, with a porosity of below 1% (Fig. 3). No voids are detected at the coating/substrate interface.

Etching shows a good particle deformation and optimal particle attachment with very low particle/particle voids.

The indentation curve of the studied coating is shown in Fig. 4.

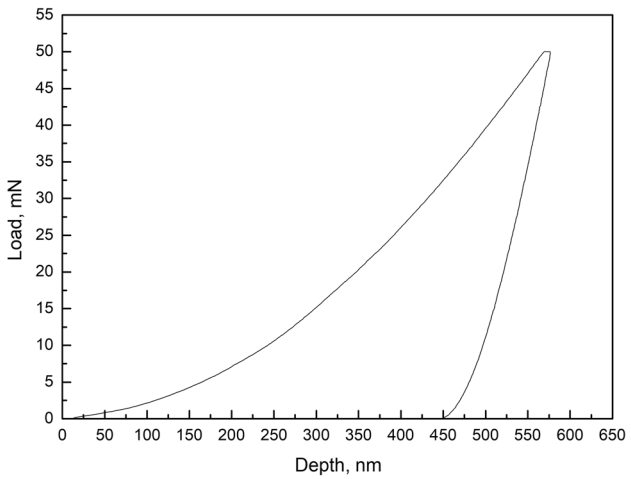

Fig. 4 Nanoindentation curve of the coating sprayed at 1000 °C and 50 bar

Furthermore, plasticity index (H/E) was calculated, because it is considered to be a reliable indicator of good wear resistance in coatings (Ref 26). Table 1 presents the calculated H/E values for 1000 °C and 50 bar coating and for 800 °C and 40 bar coating of a previous work (Ref 22). The higher the H/E ratio is, the more durable the coating can be. It can be concluded that 1000 °C and 50 bar coating shows a little bit better wear resistance $[(0.037 - 0.03)/0.037] * 100 \approx 19\%$ (Ref 27).

The increase in temperature and pressure leads to a noticeable increase in the microstructural and mechanical behavior. This aspect is immediately demonstrated by the hardness profile of the coatings if compared with the same material cold-sprayed at 800 °C and 40 bar. As a matter of fact, the hardness/modulus ratio (H/E known as plasticity index) is a key factor in the provisional behavior of wear properties of surfaces. In the present case, Young's modulus is almost constant for both the coatings while hardness increases for the coating sprayed at 1000 °C and 50 bar. This leads to a remarkable increase in the plasticity index of the material with expected increased wear resistance (Ref 26).

The 1000 °C, 50 bar and 40 mm coating has a lower corrosion current than 800 °C, 40 bar and 40 mm (Fig. 5). This could be explained to be due to lower porosity level of higher temperature and pressure coating. Porosity level can compromise the effectiveness of the coating as a barrier to corrosion current, while chromium, molybdenum and nickel confirm their protective nature of the substrate.

The coating produced at 1000 °C and 50 bar presents higher hardness with respect to the coating sprayed at 800 °C and 40 bar. In addition in the latter, the hardness values tend to decrease by moving far from the coating interface. This is due to particle tamping effect, residual stress and work hardening. Particle tamping effect affects mechanical properties of a cold-spraying coating, because subsequent particle impact onto deposited layer causes to previously deposited particles more plastic deformation and more flattened shape. Tamping effect and compression ratio R_c (Ref 28) are often used in the literature to explain and to indicate the particle deformation level. Residual stress and work hardening in cold-sprayed process decrease the mechanical properties of coatings. Work hardening generated during the impact process of particles leads to coatings with excellent tensile strength, but with low ductility (Ref 29). A more stable profile is observed for the coating cold-sprayed at 1000 °C and 50 bar (Fig. 6).

Fatigue Behavior

The aspect of the different notched specimens after fatigue tests is shown in Fig. 7.

As observed in a previous work (Ref 22), the crack propagates at the center of the notches with two additional cracks appearing on the coating surface far from the notches. These additional cracks are also probably due to a decohesion component during the fatigue loading due to the stress concentration in the final stage of the loading. In a recently published paper (Ref 30), a new specimen for axial fatigue test is proposed to assess the fatigue behavior of locally damaged parts repaired with cold spray and subjected to cyclic loading. Three different shapes of cavity embodied in the specimen representing the defect to be repaired are discussed. Here, the stress intensity factor due to the differently shaped defects was largely analyzed through FEM calculations. Obviously, the cyclic properties are strongly dependent on the residual stresses, a crucial aspect for cold spray coatings. The results belonging to the x-rays measurements are described in Fig. 8.

The crack length as a function of the number of fatigue cycles is shown in Fig. 9. For comparison, the data are plotted in comparison with those belonging to different spray conditions of coatings tested with the same fatigue parameters (load and notch geometries (Ref 22)).

The increase in spray temperature and pressure leads to increased coating hardness and to lowered porosity. Also cohesion between the particles is believed to be a crucial factor leading to the increase in fatigue properties as will

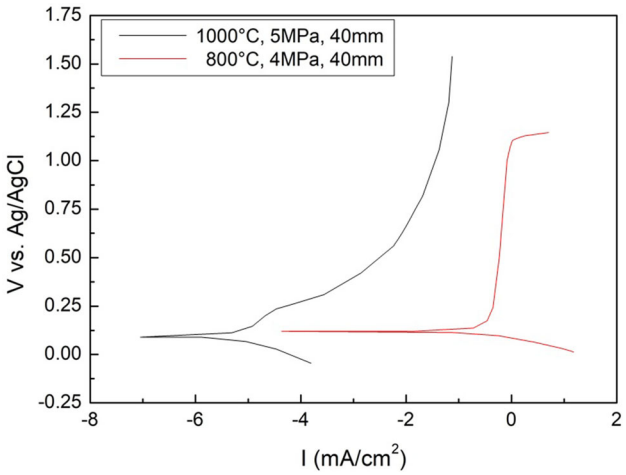

Fig. 5 Potentiodynamic polarization curves for both IN625 coatings

Table 1 H/E ratio measured for coatings

Process conditions	Indentation hardness H, GPa	Young's modulus E, GPa	H/E
1000 °C, 50 bar	8.30 ± 0.90	222 ± 11	0.037
800 °C, 40 bar	6.40 ± 0.53	212 ± 22	0.030

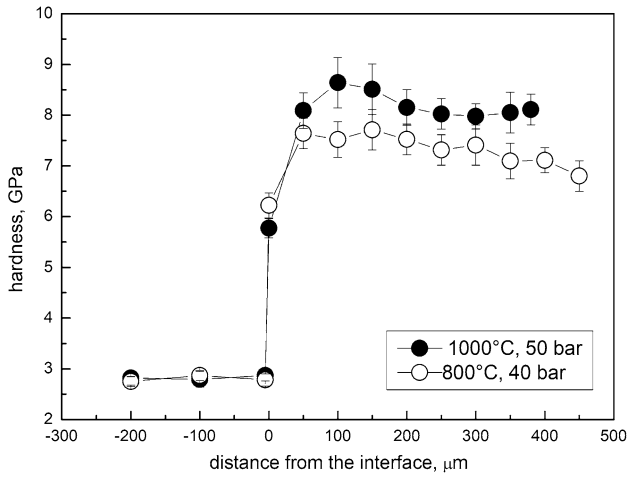

Fig. 6 Hardness profile evaluated through nanoindentation

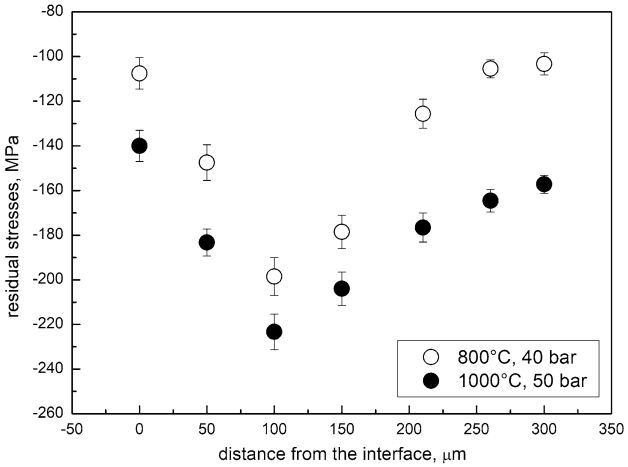

Fig. 8 Residual stresses profiles for both the cold-sprayed conditions

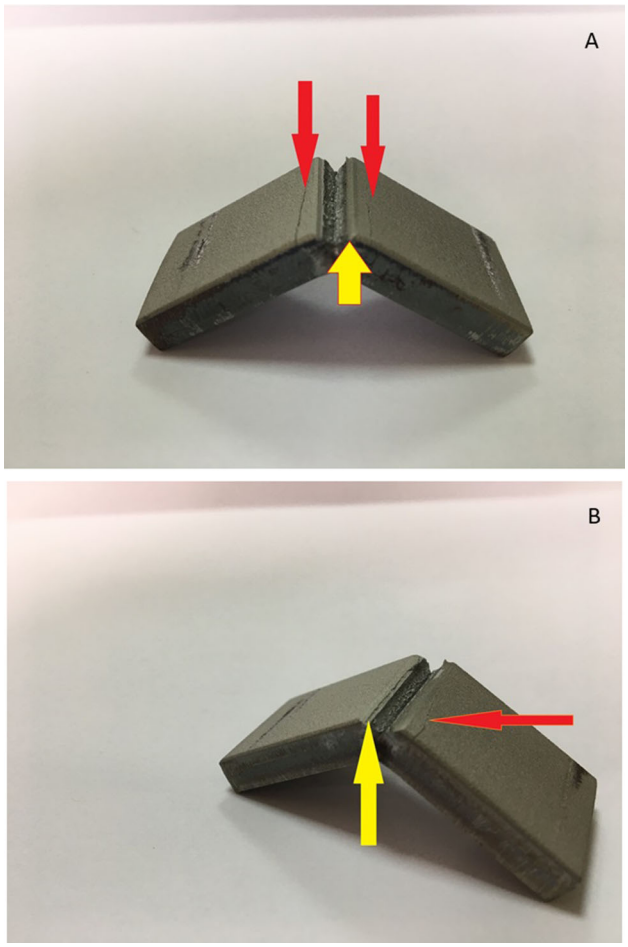

Fig. 7 Notched samples after fatigue tests, 60° notch (a); 90° notch (b)

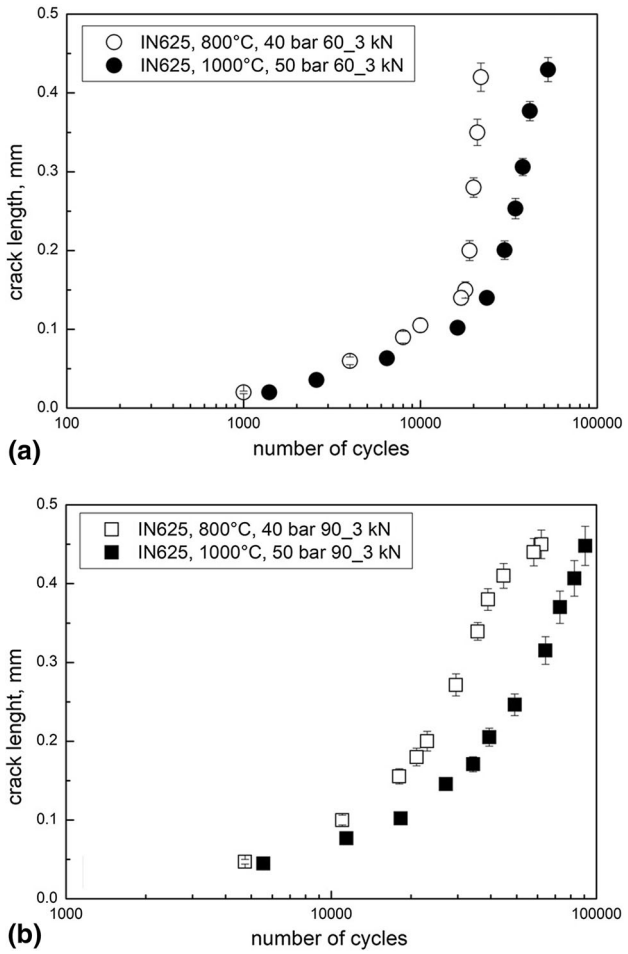

Fig. 9 Crack length as a function of the number of fatigue cycles for the tested materials and geometries, 60° notch (a); 90° notch (b)

be discussed after the fracture surface observation. The crack growth rate as a function of the applied ΔK is shown in Fig. 10.

The improvement in fatigue properties is demonstrated by the lower crack rate as a function of the same applied ΔK for the coatings sprayed to higher temperature and pressure. As expected, the crack rate is lower for the 90°

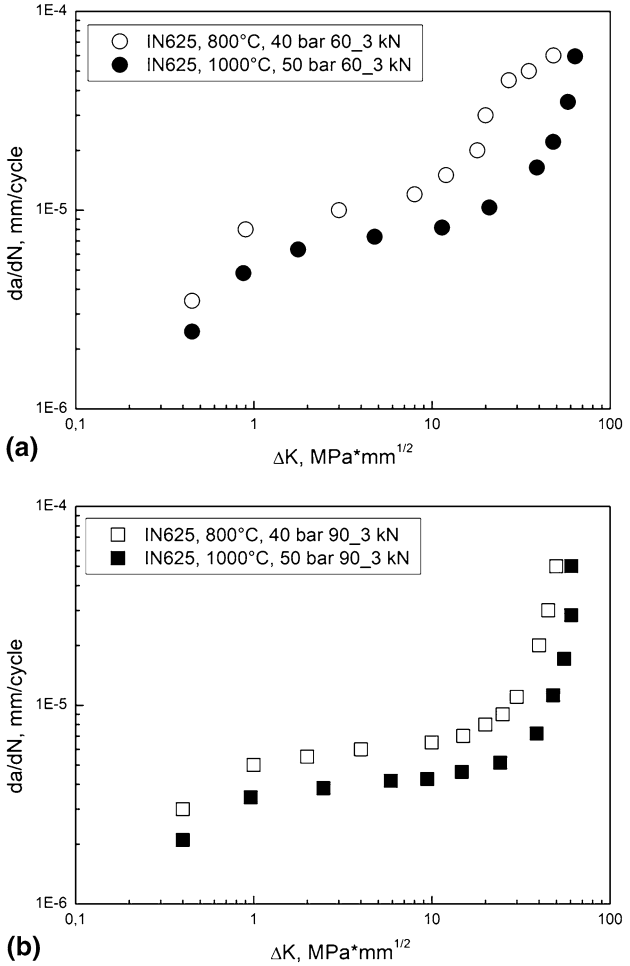

Fig. 10 Crack length as a function of the applied ΔK for all the studied coatings, 60° notch (a); 90° notch (b)

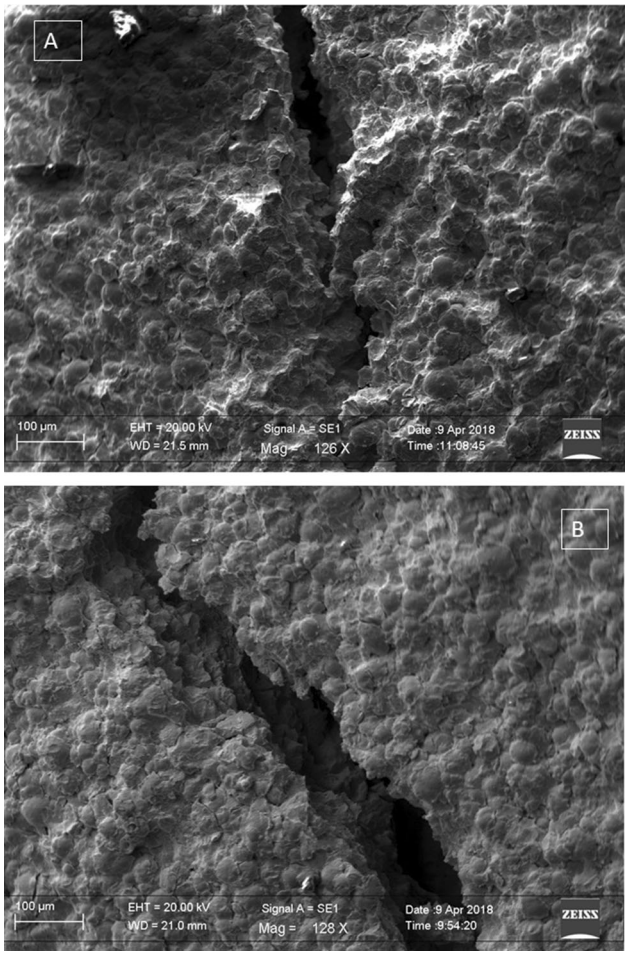

Fig. 11 Notch cracks for the specimens tested in fatigue bending, 60° notch (a); 90° notch (b)

notched samples because of the lower stress concentration due to the increased notch aperture. It is expected that particles filling the 60° notch have more difficulties in adhering with respect to the 90° notch because of the different impacting angles (Ref 31). Normally, crack initiation acts at the coating surface. When the coating/substrate strength (adhesion) is high, the propagation locates in a direction perpendicular to the coating thickness in the loading direction. When the coating/substrate strength is low, delamination occurs during cyclic loading and the first nucleated cracks do not propagate; in this case, coating decohesion is the main damage mechanism. Once local delamination acts as a consequence of delamination, the coating/substrate interface rapidly damages, decreasing the rate of further crack nucleation (Ref 32). A different mechanism leading to delamination could be the small crack coalescence during propagation in regions close to the substrate/coating interface. In the case of multiple-crack formation, their density is directly related to the interfacial strength (Ref 33). In the present case, the coating sprayed at 1000 °C and 50 bar shows a more stable crack propagation with respect to the one spayed at 800 °C and 40 bar. This behavior is attributed to lower pore presence and consequently to the different plastic regions at the crack tip. In this way, the crack propagates slowly in the case of the coating sprayed at 1000 °C and 50 bar with both the tested notch geometries (as shown in Fig. 10). Obviously, the crack growth rate increases with decreasing notch angle for both the spraying conditions.

Fracture Behavior

The fatigue crack propagates at the center of the notches, and no damage or decohesion between the particles is observed in other zones close to the main propagating crack for all the employed geometries (Fig. 11).

Previous work demonstrated that the main deformation mode of the material sprayed at 800 °C and 40 bar was decohesion between the IN625 particles with experienced local ductility. In the case of the coatings produced at

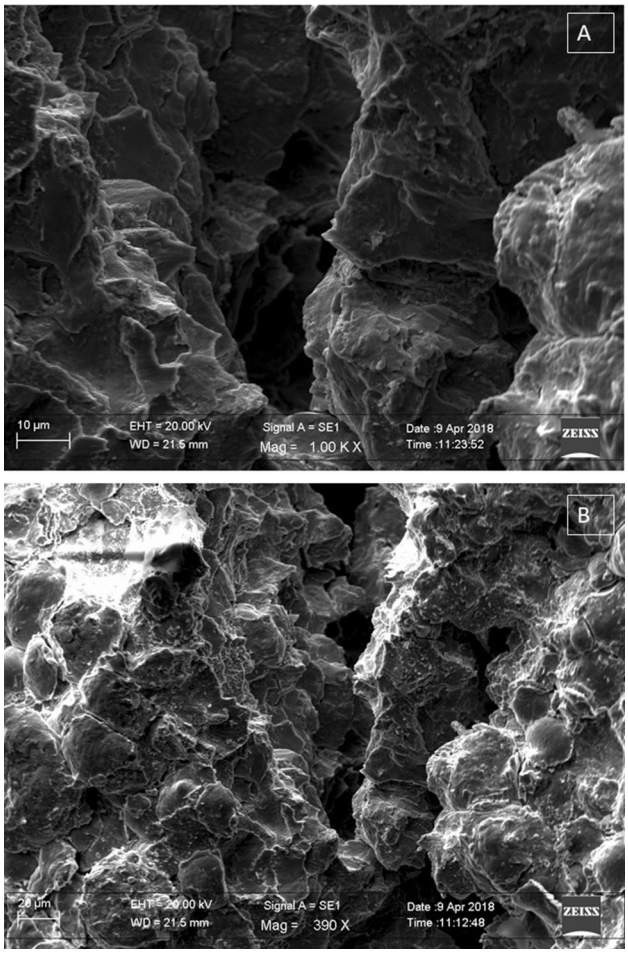

Fig. 12 Fracture surface of the 60° notched specimen sprayed at 1000 °C and 50 bar

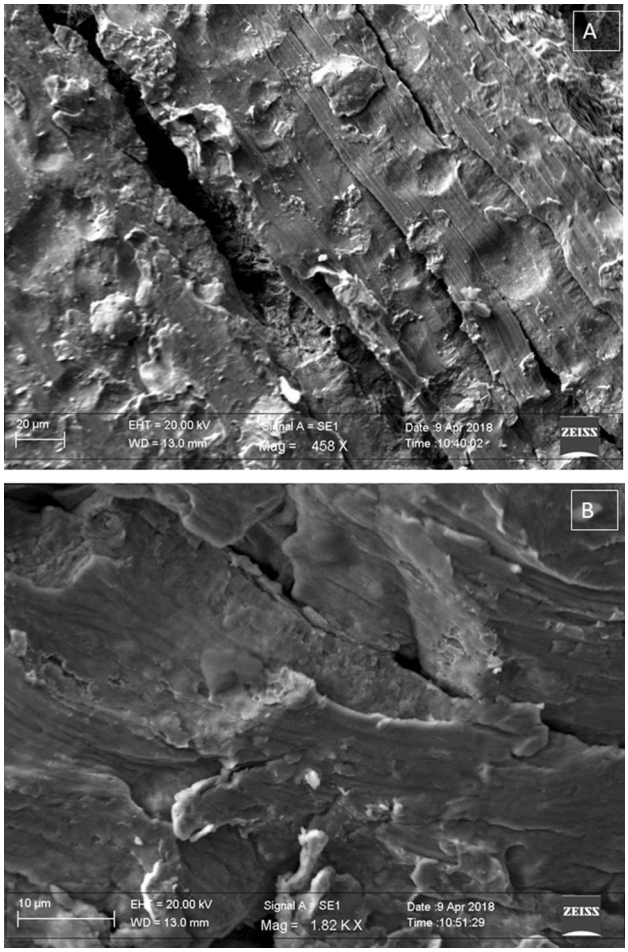

Fig. 13 Fatigue striations observed on the fracture surface of the 90° notched sample

1000 °C and 50 bar, a much more ductile deformation of the particles before fracture is observed for both the employed geometries (Fig. 12).

In the case of the observed fracture surfaces, decohesion is not the main damage mechanism in these coatings demonstrating the excellent particle/particle bonding. In addition, many fatigue striation zones were observed on the fractured surface of the specimen with 90° notch (Fig. 13). These striations were never been observed in the coatings sprayed at 800 °C and 40 bar. They form at each cycle once the material is compact and the fracture does not propagate through voids or in a transgranular or interparticle way.

As a matter of fact, the local behavior depends on both processing parameters and notch geometry (defining the stress concentration). Once the particles are sprayed at 1000 °C and 50 bar, the coatings show a more ductile cold behavior with respect to those sprayed at 800 °C and 40 bar with a crack growing with mixes of particle/particle decohesion and typical fatigue striation behavior. For the coatings sprayed at 800 °C and 40 bar, only particle/particle decohesion is observed on the crack path.

Conclusion

IN625 superalloy coatings were produced via cold spray on C steel substrate at 1000 °C and 50 bar. The coatings' mechanical properties and microstructure were compared with those produced at 800 °C and 40 bar whose properties were previously presented. At the highest spray temperature and pressure (1000 °C and 40 bar), lower levels of porosity and hardness increase were recorded. In addition, improved corrosion properties were revealed. The microstructurally and mechanically improved features led to improved fatigue properties under crack initiation and growth tests in bending. The fracture behavior revealed that the coating sprayed at 1000 °C and 50 bar showed higher plasticity and local ductility much more increased with respect to the coating sprayed at 800 °C and 40 bar.

References

1. Y. Hu, M. Madhava, and F. Renteria, Cold gas-dynamic spray repair on gas turbine engine components, United States Patent, 2005. US6905728B1.
2. K. Ogawa and D. Seo, Repair of Turbine Blades Using Cold Spray Technique, *Advances in Gas Turbine Technology*, E. Benini, Ed., InTech, 2011, https://www.intechopen.com/books/advances-in-gas-turbine-technology/repair-of-turbine-blades-using-coldspray-technique
3. J. Flannery, *It's Time to Pay Attention to AM, Metal AM*, Innovar Comunications Ltd, Shrewsbury, 2018
4. S. Yin, P. Cavaliere, B. Aldwell, R. Jenkins, H. Liao, W. Lid, and R. Lupoi, Cold Spray Additive Manufacturing and Repair: Fundamentals and Applications, *Addit. Manuf.*, 2018, **21**, p 628-650. https://doi.org/10.1016/j.addma.2018.04.017
5. P. Cavaliere, A. Perrone, and A. Silvello, Fatigue Behaviour of Inconel 625 Cold Spray Coatings, *Surf. Eng.*, 2018, **34**(5), p 380-391
6. D.R. Muzyka, *The Superalloys*, C.T. Sims and W.C. Hagel, Ed., Wiley, New York, 1972, p 113-143
7. M. Sundararaman, P. Mukhopadhyay, and S. Banerjee, Precipitation of the δ-Ni_3Nb Phase in Two Nickel Base Superalloys, *Metall. Trans. A*, 1988, **19**, p 453-465
8. E. Andrieu, N. Wang, R. Molins, and A. Pineau, in E.A. Loria (ed.) *Influence of Compositional Modifications on Thermal Stability of Alloy 718, Superalloys 718, 625 and Various Derivatives*. (TMS, 1994), p 695-710.
9. O.B. Armida and J.F. Radavich, A current T-T-T Diagram for Wrought Alloy 718, Superalloy 718, 625 and Various Derivatives. Ed. E.A. Loria, (TMS, 1991), p 325-335.
10. S.H. Fu, J.X. Dong, M.C. Zhang, and X.S. Xie, Alloy Design and Development of INCONEL718 Type Alloy, *Mater. Sci. Eng.*, 2009, **A499**(1-2), p 215-220
11. A. Silvello, *Cold Spray Coatings-Recent Trends and Future Perspective*, P. Cavaliere, Ed., Springer, Berlin, 2018, https://doi.org/10.1007/978-3-319-67183-3
12. A. Moridi, S.M. Hassani-Gangaraj, M. Guagliano, and M. Dao, Cold Spray Coating: Review of Material System and Future Perspective, *Surf. Eng.*, 2014, **36**(6), p 369-395
13. J. Henao, A. Concustell, I.G. Cano, S. Dosta, N. Cinca, J.M. Guilemany, and T. Suhonen, Novel Al-Based Metallic Glass Coatings by Cold Gas Spray, *Mater. Des.*, 2016, **94**, p 253-261
14. S. Yin, B. Aldwell, and R. Lupoi, *Cold Spray Coatings-Recent Trends and Future Perspective*, P. Cavaliere, Ed., Springer, Berlin, 2018, https://doi.org/10.1007/978-3-319-67183-3
15. D. Verdi, M.A. Garrido, C.J. Múnez, and P. Poza, Mechanical Properties of Inconel 625 Laser Cladded Coatings: Depth Sensing Indentation Analysis, *Mater. Sci. Eng. A*, 2014, **598**, p 15-21
16. IN625 Bullettin of Special Metal Company, http://www.specialmetal.com/. Accessed 13 August 2013
17. K. Petráčková, J. Kondás, and M. Guagliano, Mechanical Performance of Cold-Sprayed A357 Aluminum Alloy Coatings for Repair and Additive Manufacturing, *J. Therm. Spray Technol.*, 2017, **26**(8), p 1888-1897
18. A. Moridi, S.M. Hassani-Gangaraj, S. Vezzú, L. Trško, and M. Guagliano, Fatigue Behavior of Cold Spray Coatings: The Effect of Conventional and Severe Shot Peening as Pre-/Post-Treatment, *J. Therm. Spray Technol.*, 2015, **283**, p 247-254
19. A. Moridi, S.M. Hassani-Gangaraj, and M. Guagliano, On Fatigue Behavior of Cold Spray Coating, *J. Inst. Econ.*, 2014, **1650**(2), p 803
20. R. Ghelichi, S. Bagherifard, D. MacDonald, M. Brochu, H. Jahed, B. Jodoin, and M. Guagliano, Fatigue Strength of Al Alloy Cold Sprayed with Nanocrystalline Powders, *Int. J. Fatigue*, 2014, **65**, p 51-57
21. P. Cavaliere, *Cold-Spray Coatings-Recent Trends and Future Perspectives*, Springer, Berlin, 2018, https://doi.org/10.1007/978-3-319-67183-3
22. P. Cavaliere, A. Silvello, N. Cinca, H. Canales, S. Dosta, I. Garcia Cano, and J.M. Guilemany, Microstructural and Fatigue Behavior of Cold Sprayed Ni-Based Superalloys Coatings, *Surf. Coat. Technol.*, 2017, **324**, p 390-402
23. I.C. Noyan and J.B. Cohen, *Residual Stress—Measurement by Diffraction and Interpretation. Materials Research and Engineering*, Springer, New York, 1987
24. P. Cavaliere, Fatigue Properties and Crack Behavior of Ultra-fine and Nanocrystalline Pure Metals, *Int. J. Fatigue*, 2009, **31**, p 1476-1489
25. J. Lian, M. Sharaf, F. Archie, and S. Munstermann, A Hybrid Approach for Modelling of Plasticity and Failure Behaviour of Advanced High-Strength Steel Sheets, *Int. J. Damage Mech.*, 2013, **22**(2), p 188-218
26. A. Leyland and A. Matthews, On the Significance of the H/E Ratio in Wear Control: A Nanocomposite Coating Approach to Optimised Tribological Behaviour, *Wear*, 2000, **246**, p 1-11. https://doi.org/10.1016/S0043-1648(00)00488-9
27. A. Góral, W. Żórawski, P. Czaja, L. Lityńska-Dobrzyńska, M. Makrenek, and S. Kowalski, Effect of Powder Morphology on the Microstructure and Properties of Cold Sprayed Ni Coatings, *Int. J. Mater. Res.*, 2019, **110**(1), p 49-59
28. X.-L.- Zhou, X.-K. Wu, H.-H. Guo, J.-G. Wang, and J.-S. Zhang, Deposition Behavior of Multi-particle Impact in Cold Spraying Process, *Int. J. Min. Met. Mater.*, 2010, **17**(5), p 635-640
29. R. Huang, M. Sone, W. Ma, and H. Fukanuma, The Effects of Heat Treatment on the Mechanical Properties of Cold-Sprayed Coatings, *Surf. Coat. Technol.*, 2015, **261**, p 278-288
30. K. Petráčková, J. Kondás, and M. Guagliano, Fixing a Hole (with Cold Spray), *Int. J. Fatigue*, 2018, **110**, p 144-152
31. G. Li, X.-F. Wang, and W.-Y. Li, Effect of Different Incidence Angles on Bonding Performance in Cold Spraying, *Trans. Nonferrous Met. Soc.*, 2007, **17**(1), p 116-121
32. J.A. Nairn, Fracture Mechanics of Composites with Residual Thermal Stresses, *J. Appl. Mech.*, 1997, **64**, p 804-810
33. S.R. Kim and J.A. Nairn, Fracture Mechanics Analysis of Coating/Substrate Systems: II. Experiments in Bending, *Eng. Fract. Mech.*, 2000, **65**, p 595-607